Energy Conversion in Shape Memory Alloy Heat Engine Part II: Simulation

J. J. Zhu, N. G. Liang, W. M. Huang and K. M. Liew

Journal of Intelligent Material Systems and Structures 2001 12: 133
DOI: 10.1106/7H9E-GD5D-D3NN-B63R

Energy Conversion in Shape Memory Alloy Heat Engine Part II: Simulation

J. J. ZHU,[1] N. G. LIANG,[2†] W. M. HUANG[1]* AND K. M. LIEW[1]

[1]*Centre for Advanced Numerical Engineering Simulations, Nanyang Technological University, Singapore 639798*
[2]*LNM Institute of Mechanics, Chinese Academy of Sciences, Beijing 100080, China*

ABSTRACT: In this paper, a theoretical model proposed in Part I (Zhu et al., 2001a) is used to simulate the behavior of a twin crank NiTi SMA spring based heat engine, which has been experimentally studied by Iwanaga et al. (1988). The simulation results are compared favorably with the measurements. It is found that (1) output torque and heat efficiency decrease as rotation speed increase; (2) both output torque and output power increase with the increase of hot water temperature; (3) at high rotation speed, higher water temperature improves the heat efficiency. On the contrary, at low rotation speed, lower water temperature is more efficient; (4) the effects of initial spring length may not be monotonic as reported. According to the simulation, output torque, output power and heat efficiency increase with the decrease of spring length only in the low rotation speed case. At high rotation speed, the result might be on the contrary.

INTRODUCTION

SHAPE memory materials have gained recognition in recent years. Usually, these materials can recover an initially designed shape upon experiencing, for instance, a temperature change. Among others, Shape Memory Alloy (SMA) is outstanding. Given a recoverable strain up to 6% and an actuation stress of 400 MPa, the potential applications of NiTi SMA are numerous.

One of the applications is heat engine. SMA based heat engine is an environment friendly alternative to extract mechanical energy from low-grade energies, such as, warm wastewater, geothermal energy, solar thermal energy, etc. Other novel applications based on the exactly same principle include motors for outer space missions.

Literature review shows the lack of efficient tool to simulate the behavior of SMA heat engines. It was reported that, in terms of efficiency, the difference between experiment and analysis might be of an order of magnitude (Funakubo, 1987).

The aim of this paper is to apply the theoretical model present in Part I (Zhu et al., 2001a) to simulate the behavior of a twin crank NiTi spring based heat engine. This heat engine has been experimentally studied by Iwanaga et al. (1988). We will use their experimental result as benchmark to verify the proposed model, and in the mean time, to explore the possibility to improve the efficiency of SMA based heat engine by various means.

*Author to whom correspondence should be addressed.
E-mail: mwmhuang@ntu.edu.sg,
†E-mail: lng@lnm.imech.ac.cn

TWIN CRANK HEAT ENGINE

The TiNi based twin crank heat engine investigated in this paper is schematically shown in Figure 1 (Iwanaga et al., 1988). This heat engine is actuated by NiTi helical springs. Each spring connects two cranks mounted on two crank axes. The operation principle is schematically shown in Figure 2. The original length of NiTi spring is shorter than the minimum length between two cranks. Since NiTi spring contracts upon heating (in hot water), the connecting points are pulled closer. In air (cooling is enhanced by an electric fan), NiTi spring cools down. Thus, it intends passively to extend. The ambient temperature was 12–15°C.

In the tested configuration, six cranks, instead of four cranks as shown in Figure 1, were used. They were arranged at angles of 60° on each crank axis. The maximum length of NiTi spring is $L_{\max} = 245$ mm, and the minimum length is $L_{\min} = 85$ mm. The mean diameter of spring is $D = 7$ mm. The spring is made of NiTi wire with a diameter d of 0.75 mm. The reported austenite finish temperature A_f of NiTi wire is 41°C. But, from the context, it seems that this was measured before heat-treatment (to memorize the close-wound spring shape). Hence, this value cannot be used in the simulation.

1045-389X/01/02 0133-8 $10.00/0 DOI: 10.1106/7H9E-GD5D-D3NN-B63R

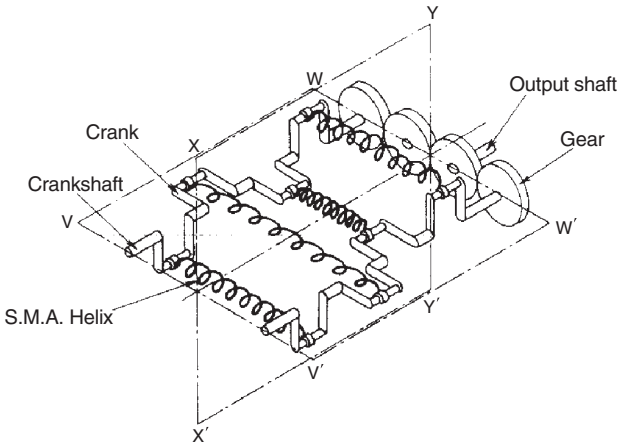

Figure 1. *Schematic diagram of twin crank SMA heat engine (Iwanaga et al., 1988).*

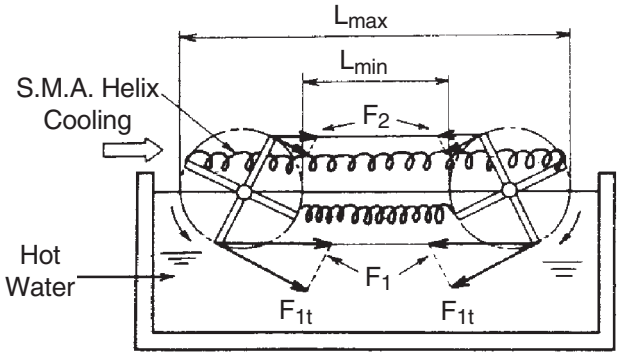

Figure 2. *Operation principle of twin crank SMA heat engine (Iwanaga et al., 1988).*

SIMULATION METHOD

If NiTi spring has n_0 turns, the initial length of a close-wound spring is given by

$$L_0 = n_0 d \tag{1}$$

Approximately, the total length of TiNi wire is

$$l_0 = \pi n_0 D \tag{2}$$

In close-wound spring, the deformation is dominated by torsion. Other deformations may be ignored for simplicity.

Given the twist angle per unit length of SMA wire as θ, the relative rotation angle of a dl long NiTi wire is

$$d\psi = \theta dl \tag{3}$$

The corresponding spring deflection is

$$d\delta = \frac{D}{2} d\psi = \frac{D}{2}\theta dl \tag{4}$$

Thus, the total deformation of NiTi spring is expressed by

$$\delta = \frac{D}{2}\int_0^{l_0} \theta dl = \frac{D}{2}\theta l_0 = \frac{1}{2} n_0 \pi D^2 \theta \tag{5}$$

That is

$$\theta = \frac{2\delta}{n_0 \pi D^2} \tag{6}$$

The spring length L in term of rotation angle φ is given by (Figure 3)

$$L = \frac{L_{\max} + L_{\min}}{2} - \frac{L_{\max} - L_{\min}}{2}\cos\varphi \tag{7}$$

Substituting Equation (1) into Equation (6) yields

$$\theta = \frac{2\delta}{n_0 \pi D^2} = \frac{2(L - L_0)}{n_0 \pi D^2} = \frac{2d}{\pi D^2}\left[\frac{L - L_0}{L_0}\right] \tag{8}$$

Substituting Equation (7) into Equation (8) gives

$$\theta = \frac{2d}{\pi D^2}\left[\frac{(L_{\max} + L_{\min}) - 2L_0}{2L_0} - \frac{(L_{\max} - L_{\min})}{2L_0}\cos\varphi\right] \tag{9}$$

The shear strain in NiTi wire is

$$\gamma = \tfrac{1}{2} r\theta; \quad 0 < r < R \tag{10}$$

where $R = \frac{1}{2} d$ is the radii of TiNi wire. Substituting Equation (9) into Equation (10) results in

$$\gamma = \frac{rd}{\pi D^2}\left[\frac{(L_{\max} + L_{\min}) - 2L_0}{2L_0} - \frac{(L_{\max} - L_{\min})}{2L_0}\cos\varphi\right] \tag{11}$$

Given tension force P and torque M, the shear stress may be expressed as $\tau = \tau(r, \gamma)$. Thus,

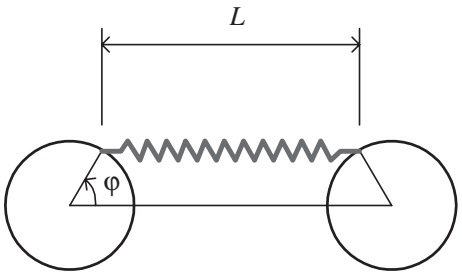

Figure 3. *Relationship between spring length and rotation angle of crank.*

$$P\frac{D}{2} = M = \int_{\Omega} \tau(r,\gamma)\, r d\Omega = 2\pi \int_0^R \tau(r,\gamma) r^2 dr \qquad (12)$$

Because NiTi wire is thin and the whole spring immerses into and comes out of the hot water in the same time, we may assume the temperature of each NiTi spring is uniform everywhere.

To simulate the thermo-mechanical behavior of TiNi spring, a simplified model proposed by Zhu et al. (2001a) is applied. Readers may refer to Zhu et al. (2001a) for the details of derivation and the meanings of various symbols.

Consider a unit length of NiTi wire and ignoring heat source term, i.e., let $\dot{r} = 0$ in Equation (62) of Zhu et al. (2001a). Then, Equation (62) of Zhu et al. (2001a) yields

$$\pi R^2 C_V \dot{T} = 2\pi R\alpha (T_W - T) + \frac{2\pi}{N_0} \int_0^R \left[\sum_{k=1}^{N_0} (\Pi_k - \Delta h T)\dot{z}_k \right] r dr \qquad (13)$$

or

$$\dot{T} = \frac{2\alpha}{\mathrm{R} C_V}(T_W - T) + \frac{2}{\mathrm{R}^2 C_V N_0} \int_0^R \left[\sum_{k=1}^{N_0} (\Pi_k - \Delta h T)\dot{z}_k \right] r dr \qquad (14)$$

If the crank rotates at a constant angular velocity ω, the rotation angle is $\varphi = \omega t$. Thus $d/dt = \omega d/d\varphi$. Rewriting Equation (14) as

$$\frac{dT}{d\varphi} = \frac{2\alpha}{\omega R C_V}(T_W - T) + \frac{2}{R^2 C_V N_0} \int_0^R \left[\sum_{k=1}^{N_0} (\Pi_k - \Delta h T)\frac{dz_k}{d\varphi} \right] r dr \qquad (15)$$

The thermo-dynamic driving force corresponding to martensite volume fraction z_k is given by (Zhu et al., 2001a)

$$\Pi_k = \Sigma \mathbf{:}\, \mathbf{E}_k + (T\Delta h - \Delta u) - A(1 - 2z_k) \qquad (16)$$

where

$$\mathbf{E}_k = g\mathbf{P}_k = \frac{g}{2}(\mathbf{m}_k \otimes \mathbf{n}_k + \mathbf{n}_k \otimes \mathbf{m}_k) \qquad (17)$$

Here, $\mathbf{n}_k$ is normal direction of habit plane of orientation component k, $\mathbf{m}_k$ is shear direction, and g is the magnitude of shear.

The critical condition for phase transformation start is

$$\Pi_k = \Pi_k^{c\pm}, \quad (k = 1,2,\ldots N_0) \qquad (18)$$

And the evolution equation of phase transformation is

$$\left.\begin{array}{ll} \dot{\Pi}_k = \dot{\Pi}_k^{c+} = 2\lambda \dot{z}_k^* & \text{for forward transformation} \\ \dot{\Pi}_k = \dot{\Pi}_k^{c-} = 2\lambda \dot{z}_k^* & \text{for reverse transformation} \end{array}\right\} \qquad (19)$$

The evolution equation may be rewritten as

$$\frac{d\Sigma}{d\varphi} : \mathbf{E}_k + \frac{dT}{d\varphi}\Delta h = 2(\lambda - A)\frac{dz_k}{d\varphi} \qquad (20)$$

RESULTS AND DISCUSSIONS

Table 1 lists the parameters used in the simulation. Four transformation temperatures can be measured by differential scanning calorimeter test. ε_0 may be determined by uni-axial test as described in Zhu et al. (2001b). Numerical simulations and experimental measurements are shown in Figures 4–22. Among them, Figures 4–6 show our simulation results and the test results reported in Iwanaga et al. (1988). Additional simulation results, without experimental comparison, are plotted in Figures 7–22.

Table 1. Parameters used in simulation.

Symbol	Designation	Value	Unit
$L_{\max}$	Maximum spring length	245	mm
$L_{\min}$	Minimum spring length	85	mm
D	Diameter of spring	7	mm
d	Diameter of NiTi wire	0.75	mm
n_0	Number of turns of NiTi spring	40, 44, 48	
E	Elastic modulus	40	GPa
ν	Poisson ratio	0.3	
C_V	Specific heat of NiTi	2.0	MK/m^3
α	Heat exchange coefficient	4000.0	W/m^2/K
M_f	Martensite finish temperature	253.0	K
M_s	Martensite start temperature	263.0	K
A_s	Austenite start temperature	273.0	K
A_f	Austenite finish temperature	283.0	K
ε_0	Tension parameter	0.4	
T_1	Tensile test temperature 1	285	K
T_2	Tensile test temperature 2	253	K
σ_1	NiTi wire yield stress at T_1	200	MPa
σ_2	NiTi wire yield stress at T_2	400	MPa
$\frac{\Delta\sigma}{\Delta T}$	$\frac{\Delta\sigma}{\Delta T} = \frac{(\sigma_2 - \sigma_1)}{(T_2 - T_1)}$	5.0	MPa/K
Δh	$-\frac{\Delta\sigma}{\Delta T}\cdot\varepsilon_0$	−2.0	MPa/K
Δu	$\frac{1}{2}(A_s + M_s)\,\Delta h$	−516.0	MPa
A	$-0.1 \times \frac{(A_s - M_s)}{2}\Delta h$	1.0	MPa
Π_0	$-0.9 \times \frac{(A_s - M_s)}{2}\Delta h$	9.0	MPa
λ	$A - \frac{[(A_f + M_s) - (A_s + M_f)]}{4}\Delta h$	11.0	MPa

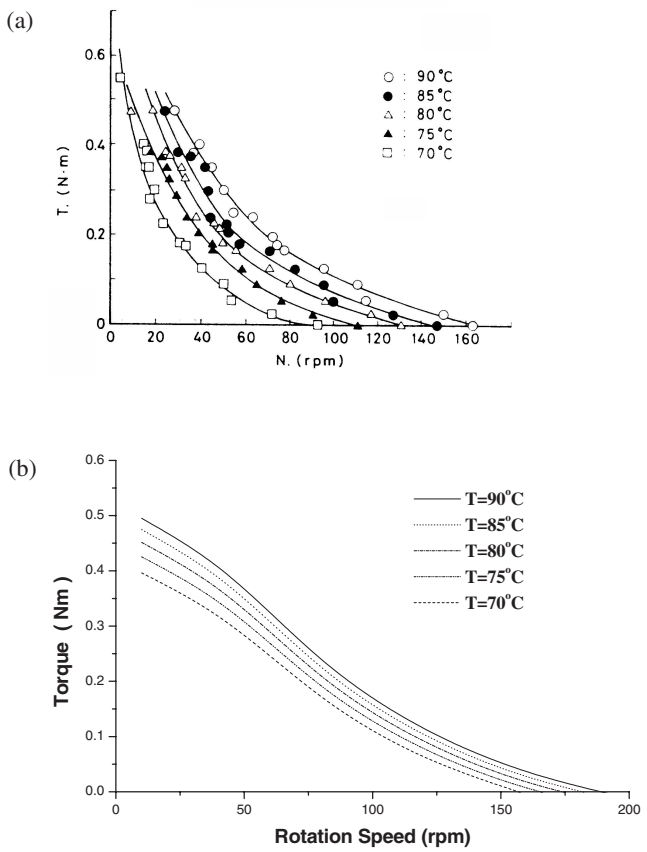

Figure 4. *Relationship between output torque and rotation speed. (a) Experiment (Iwanaga et al., 1988); (b) numerical simulation.*

It should be pointed out that, since we cannot obtain experimental values for every required parameter from the literature (Iwanaga et al., 1988), for instance, the transformation temperatures of NiTi SMA, some differences between numerical simulation and experiment are expected.

Figure 4 shows the curves of output torque versus rotation speed at different water temperatures. In general, both test and simulation share the same trend, i.e., the reduced torque accompanied with the increase of rotation speed, except at very low rotation speed.

Figure 5 shows the output power versus rotation speed curves. As we can see, all the curves are virtually convex, and the output power reaches the maximum at a certain rotation speed. Numerical simulation shows a slightly higher output power than that obtained in experiment. But the difference is much less than an order of magnitude. If we also consider friction, which may *eat* up part of the output power, we may expect an even better result.

The influence of initial NiTi spring length on the output power is plotted in Figure 6. In general, given the same initial length, a similar trend is found in both test and simulation. The apparent difference in $L_0 = 15\,\text{mm}$ case will be explained later.

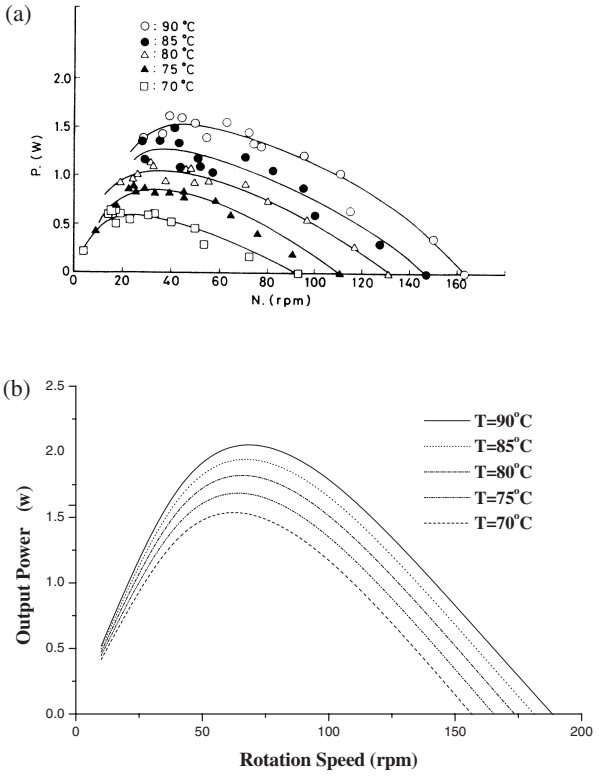

Figure 5. *Relationship between output power and rotation speed. (a) Experiment (Iwanaga et al., 1988); (b) numerical simulation.*

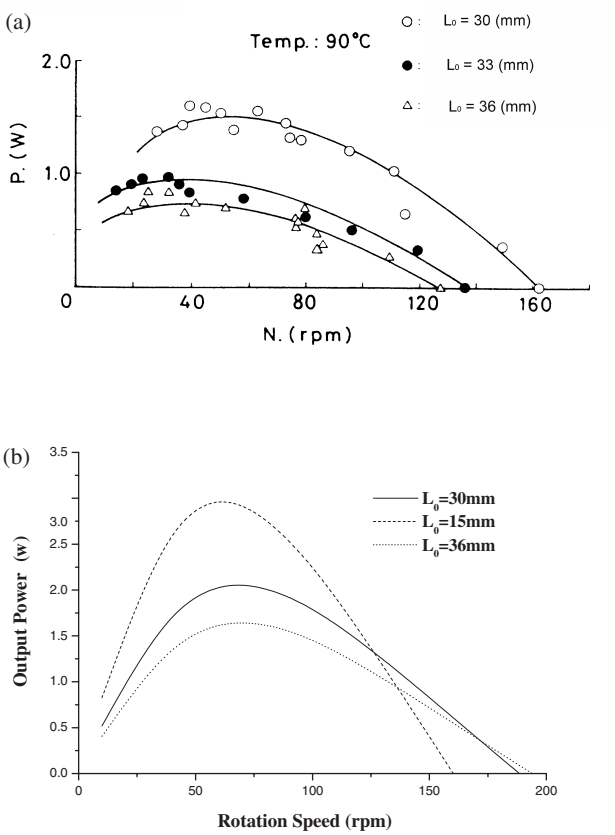

Figure 6. *Influence of initial spring length on output power. (a) Experiment (Iwanaga et al., 1988); (b) numerical simulation.*

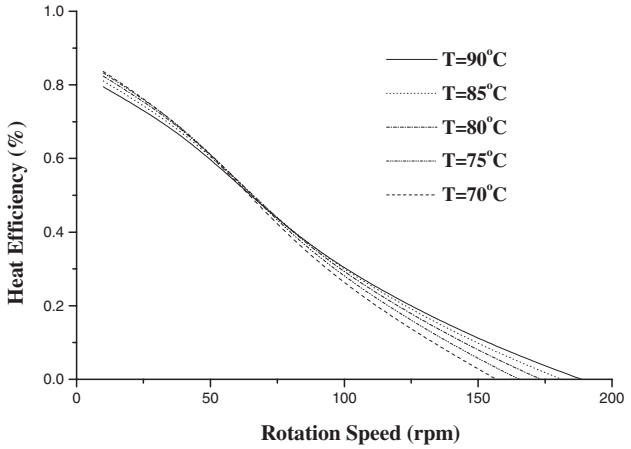

Figure 7. *Relationship between heat efficiency and rotation speed.*

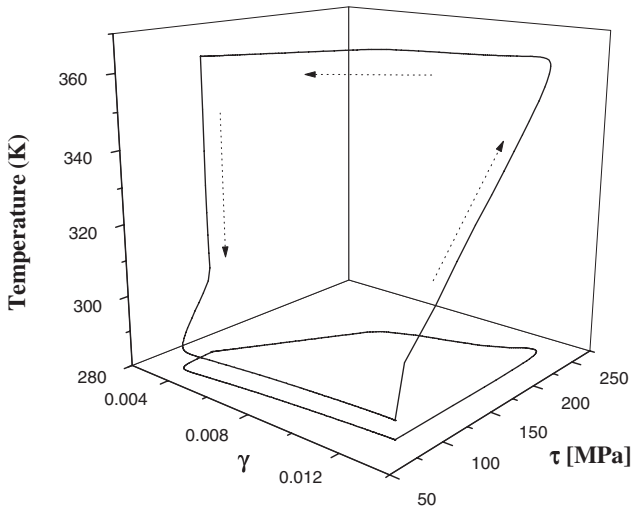

Figure 8. *Maximum shear stress–maximum shear strain–temperature relationship at* $\omega = 10$ (r.p.m) *and water temperature* $T = 90°C$.

Heat efficiency decreases as rotation speed increases, despite the difference of hot water temperature, which ranges from 70°C to 95°C. This is observed in Figure 7. At about 62.5 r.p.m, different water temperatures have almost the same heat efficiency of about 0.45%. At a lower rotation speed, cooler water temperature is more efficient. On the other hand, at a higher rotation speed, the efficiency of heat engine is improved by the increase of water temperature. The maximum heat efficiency is always less than 1%.

We can obtain 3-D plots of maximum shear stress – maximum shear strain – temperature relationship (Figures 8–11) and their projections onto shear stress – shear strain plane (Figures 12–15) at various rotation speeds. Figure 16 shows the maximum shear stress – maximum shear strain – rotation speed relationship. We can see that in each cycle, the maximum shear strain in NiTi SMA is only about 1.3%. Taking elastic strain out, the real phase transformation strain is less than 1%.

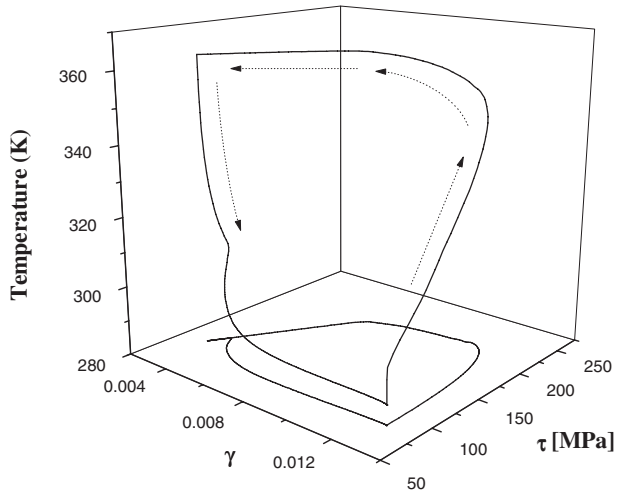

Figure 9. *Maximum shear stress–maximum shear strain–temperature relationship at* $\omega = 40$ (r.p.m) *and water temperature* $T = 90°C$.

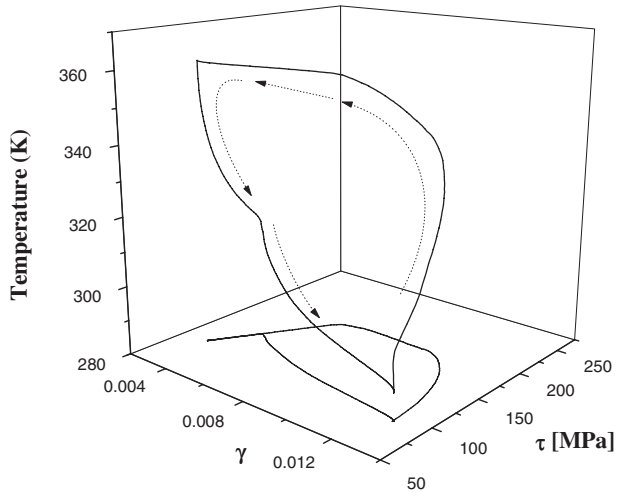

Figure 10. *Maximum shear stress–maximum shear strain–temperature relationship at* $\omega = 80$ (r.p.m) *and water temperature* $T = 90°C$.

Considering the fact that phase transformation strain of non-textured polycrystalline TiNi, which is the main contributor to the recovery strain, is about 6%, it is apparent that, in this design, the potential of NiTi SMA is not fully utilized.

In fact, the efficiency of heat engine depends on the area encircled by shear strain vs. shear stress curve in one complete cycle as shown in Figures 12–15. Given a particular configuration and water temperature, at high rotation speed the area is smaller, while at low rotation speed the area is much larger (Figures 12–15). This is consistent with the general trend of efficiency vs. rotation speed relationship.

Provided that fatigue is not a problem, higher efficiency is achievable by the use of larger phase transformation strain.

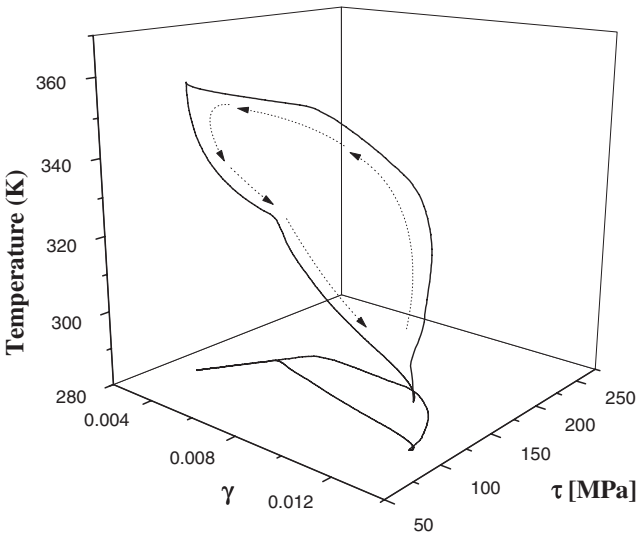

Figure 11. *Maximum shear stress–maximum shear strain–temperature relationship at* $\omega = 120$ (r.p.m) *and water temperature* $T = 90°C$.

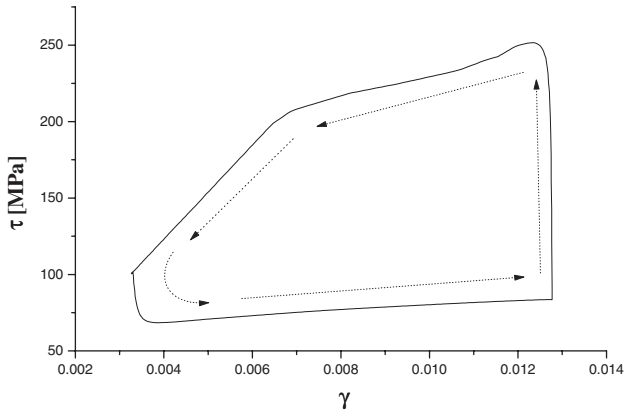

Figure 12. *Relationship between maximum shear stress and maximum shear strain at* $\omega = 10$ (r.p.m) *and water temperature* $T = 90°C$.

There are two ways to implement higher transformation strain in SMA. One is to increase the distance between two cranks, and the other is to reduce the initial length of SMA spring. In our numerical simulation, the latter method is adopted, since it was also chosen by Iwanaga et al. (1988). In experiment, three initial spring lengths of 30, 33 and 36 mm were used. In numerical simulation, three initial spring lengths, i.e., 15, 30 and 36 mm, are considered in order to investigate the effect of initial spring length in a larger range.

As shown in Figure 6(b) and Figures 17–18, given water temperature 90°C, the initial spring length does affect the output power, output torque and heat efficiency significantly. As expected, a shorter spring improves the heat efficiency tremendously. The efficiency of 15 mm spring is over 2.2% at a rotation speed of 10 r.p.m (Figure 17), which is almost three times higher than that of 36 mm spring. But a closer look shows that such effect is limited to low rotation speed (< 150 r.p.m in this studied case). At a higher rotation speed (> 150 r.p.m), the efficiency of short spring actually decreases significantly. Similar trend applies to the output torque (Figure 18) and output power [Figure 6(b)].

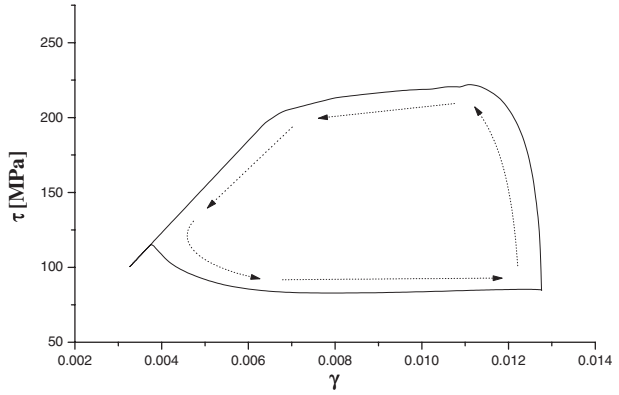

Figure 13. *Relationship between maximum shear stress and maximum shear strain at* $\omega = 40$ (r.p.m) *and water temperature* $T = 90°C$.

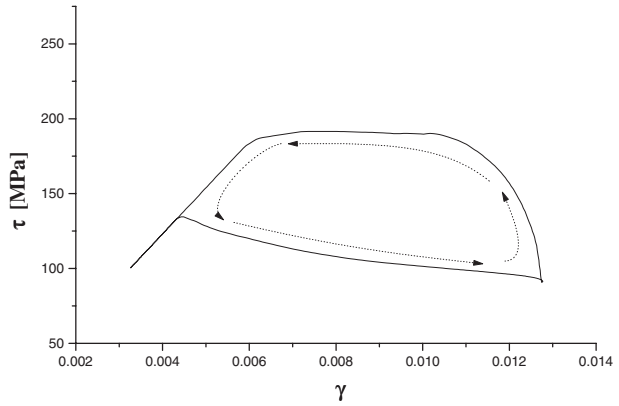

Figure 14. *Relationship between maximum shear stress and maximum shear strain at* $\omega = 80$ (r.p.m) *and water temperature* $T = 90°C$.

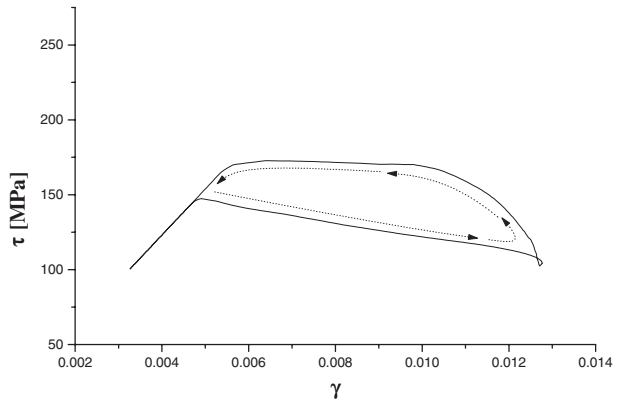

Figure 15. *Relationship between maximum shear stress and maximum shear strain at* $\omega = 120$ (r.p.m) *and water temperature* $T = 90°C$.

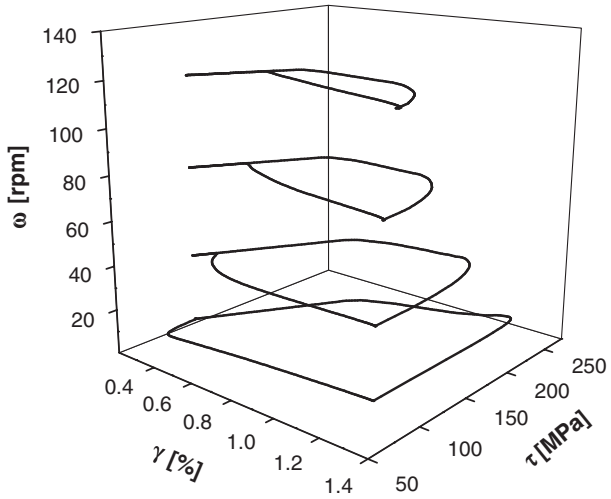

Figure 16. *Maximum shear stress–maximum shear strain–rotation speed relationship.*

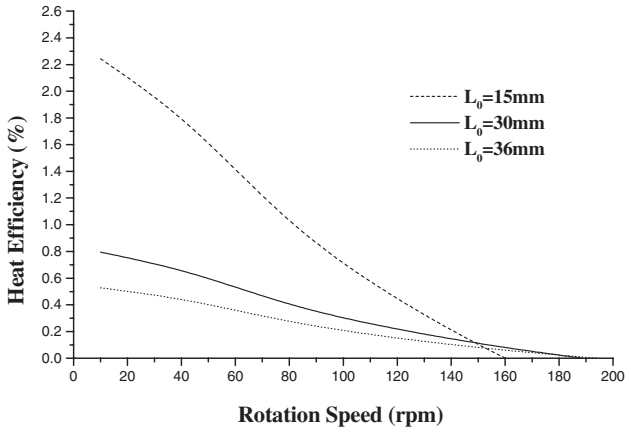

Figure 17. *Influence of initial spring length on heat efficiency. Temperature of hot water $T = 90^{\circ}$C.*

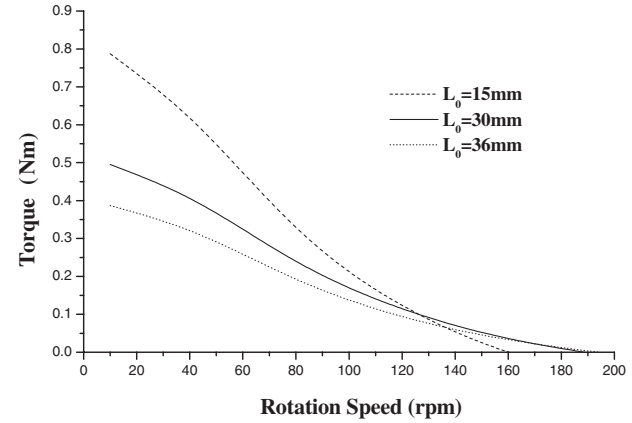

Figure 18. *Influence of initial spring length on output torque at water temperature $T = 90^{\circ}$C.*

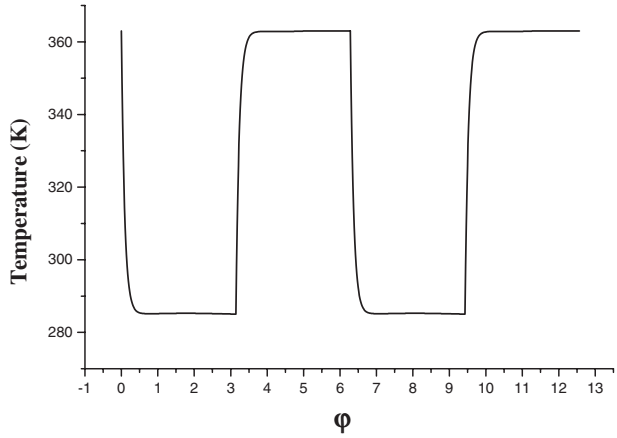

Figure 19. *Relationship between spring temperature and rotation angle of crank at $\omega = 10$ (r.p.m) and water temperature $T = 90^{\circ}$C.*

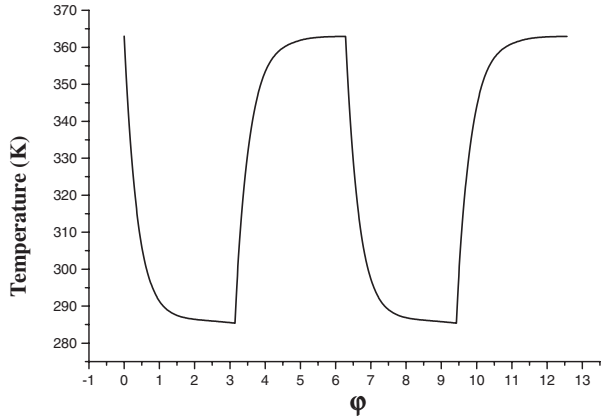

Figure 20. *Relationship between spring temperature and rotation angle of crank at $\omega = 40$ (r.p.m) water temperature $T = 90^{\circ}$C.*

On comparison with the experimental result shown in Figure 6(a), where the effect of initial spring length on output power is monotonic over the all tested rotation speed range, it seems that our result is on the contrary to what had happened in the real heat engine at high rotation speed. Recall Figure 6(b), the significant decrease is observed in which the initial spring length is 15 mm, while the difference between initial lengths of 30 and 36 is small. This provides a possible explanation. That is: what observed in the experiment is only part of the picture. When the initial spring length is reduced significantly, we may obtain the same phenomenon as shown in Figure 6(b).

Figures 19–22 show the relationships of wire temperature vs. rotation angle at different rotation speeds. As we can see, in all cases, the highest temperature reached in SMA is almost the same at all speeds. However, the lowest temperature is different. The higher the rotation speed, the higher the lowest temperature. And more importantly, the temperature–rotation angle curve is more like a zigzag. This provides further explanation for lower heat efficiency at higher speed. As the lowest temperature reached upon cooling is higher, the stress in SMA is higher. The difference

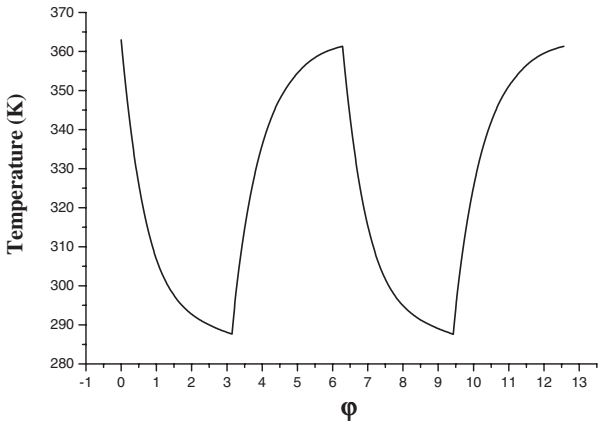

Figure 21. *Relationship between spring temperature and rotation angle of crank at* $\omega = 80$ (r.p.m) *and water temperature* $T = 90^{\circ}$C.

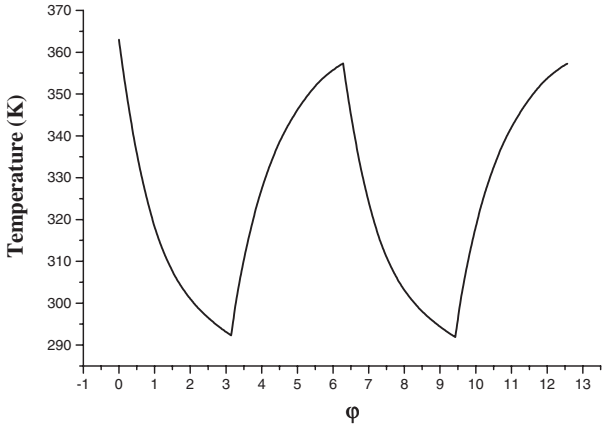

Figure 22. *Relationship between spring temperature and rotation angle of crank at* $\omega = 120$ (r.p.m) *and water temperature* $T = 90^{\circ}$C.

between high stress (in heating part) and low stress (in cooling part) is smaller. Referring to Figures 12–15, the area enclosed by strain–stress curve in one cycle is also smaller.

CONCLUSIONS

Based on the theoretical model developed in Part I, a simulation on a twin crank NiTi SMA spring based heat engine was conducted.

The information provided by Iwanaga et al. (1988) is insufficient to provide all the required parameters. Taking this fact into consideration, the simulation results are generally consistent with what were reported in Iwanaga et al. (1988). The difference is far less than "*an order of magnitude*" as reported in Funakubo (1987). It proves that the model used here is promising.

The following phenomena are observed in our simulation, which, if applicable, share the same trend with the real one:

1. Output torque and heat efficiency decrease as rotation speed increase.
2. Output power vs. rotation speed curve is convex.
3. Both output torque and output power increase with the increase of hot water temperature.
4. At high rotation speed, higher water temperature improves the heat efficiency. On the contrary, at low rotation speed, lower water temperature is more efficient. This predicated phenomenon has not been proved experimentally yet.
5. The effects of initial spring length may not be monotonic as reported. According to the simulation, output torque, output power and heat efficiency increase with the decrease of spring length only in the low rotation speed case. At high rotation speed, the result might be on the contrary.

According to simulation results present above, the efficiency of the SMA heat engine is very small (the maximum is 2–3%). This is because the strain and stress distribution upon torsion is much less efficient as compared with that upon uni-axial tension. Therefore, an SMA heat engine using axial stretching of SMA wires would be expected to have a much better efficiency.

REFERENCES

Funakubo, H. (1987). *Shape memory alloys*. Gorden and Breach Science Publishers.

Iwanaga, H., Tobushi, H. and Ito, H. (1988). Basic research on output power characteristics of a shape memory alloy heat engine. *JSME Int. J.*, Series I, **31**:634–637.

Zhu, J. J., Liang, N. G., Liew, K. M. and Huang, W. M. (2001a). Energy conversion in shape memory alloy heat engine. Part I: Theory. *J. Intell. Mater. Syst. Struct.*, **12**: 127–132.

Zhu, J. J., Liang, N. G., Huang, W. M., Liew, K. M. and Liu, Z. H. (2001b). A thermodynamic constitutive model for stress induced phase transformation in shape memory alloys. *Int. J. Solids Struct.* (in press).